

## Emergence of charge order in extremely underdoped $\text{Bi}_2\text{Sr}_{2-x}\text{La}_x\text{CuO}_{6+\delta}$

Shilong Zhang<sup>1,\*</sup>, Qizhi Li<sup>1,\*†</sup>, Changwei Zou<sup>1</sup>, Hsiao-Yu Huang<sup>2</sup>, Amol Singh<sup>2,3</sup>, Hongtao Yan<sup>4</sup>, Xingjiang Zhou<sup>4</sup>, Di-Jing Huang<sup>2</sup> and Yingying Peng<sup>1,5,‡</sup>


<sup>1</sup>*International Center for Quantum Materials, School of Physics, Peking University, Beijing 100871, China*

<sup>2</sup>*National Synchrotron Radiation Research Center, Hsinchu 30076, Taiwan*

<sup>3</sup>*Department of Physics and Astrophysics, University of Delhi, New Delhi 110007, India*

<sup>4</sup>*Beijing National Laboratory for Condensed Matter Physics, Institute of Physics, Chinese Academy of Sciences, Beijing 100190, China*

<sup>5</sup>*Collaborative Innovation Center of Quantum Matter, Beijing 100871, China*

 (Received 5 February 2024; revised 25 July 2024; accepted 20 August 2024; published 3 September 2024)

Charge order (CO) is ubiquitous in high- $T_c$  cuprate superconductors and is considered to compete with superconductivity in the underdoped region. However, how CO emerges from antiferromagnetic parent compounds is rarely studied and remains elusive. The existence of CO in extremely underdoped  $\text{Bi}_2\text{Sr}_{2-x}\text{La}_x\text{CuO}_{6+\delta}$  (La-Bi2201) has only been observed by scanning tunneling microscopy, lacking comprehensive bulk evidence. Here, we use Cu  $L_3$ -edge resonant inelastic x-ray scattering to investigate the emergence of CO in insulating La-Bi2201 samples. Our findings reveal the absence of CO at doping  $p = 0.03$ , while it becomes evident at  $p = 0.07$ . The CO diminishes with increasing temperature, with an onset temperature around 270 K, similar to the behavior of charge order in underdoped and optimally doped Bi2201. These findings suggest that CO in La-Bi2201 forms a truncated dome-shaped phase diagram as doping decreases. This phase diagram originates from the inhomogeneity of the charge distribution, where localized regions of high charge density allow CO to exist at higher temperatures. The rapid reduction of these high-density regions accounts for the disappearance of CO at lower doping levels. Our findings provide bulk evidence of CO in extremely underdoped Bi2201 and reveal how CO emerges in inhomogeneous systems.

DOI: [10.1103/PhysRevB.110.125108](https://doi.org/10.1103/PhysRevB.110.125108)

### I. INTRODUCTION

Doping electron or hole carriers into the cuprates induces the transition from a Mott insulator to superconductor [1–3]. Several quantum phases emerge in this strongly correlated system, including antiferromagnetism (AFM), pseudogap (PG), and superconductivity (SC). Unraveling the origin and relationship of these intertwined orders is crucial to understanding the mechanisms underlying high- $T_c$  superconductors. Lately, advances in x-ray sources [4] and technologies have allowed the observation of charge order (CO) in numerous cuprate families, such as  $\text{La}_{2-x}\text{Ba}_x\text{CuO}_4$  [5–9],  $\text{YBa}_2\text{Cu}_3\text{O}_7$  [10–14],  $\text{Bi}_2\text{Sr}_2\text{CuO}_{6+\delta}$  [15,16],  $\text{Bi}_2\text{Sr}_2\text{CaCu}_2\text{O}_{8+\delta}$  [17,18], and  $\text{HgBa}_2\text{CuO}_{4+\delta}$  [19]. It is widely observed that CO forms above  $T_c$  and is subsequently suppressed after entering the SC state [20–22]. Moreover, the intensity of CO would recover if Cooper pairs are destroyed by a magnetic field [20] or optical pump [23], suggesting a competing relationship between CO and SC. Therefore, the investigation of CO properties is important for understanding cuprates and unconventional superconductivity.

Although CO is universally observed in cuprates, its properties, such as wave vector, coherence length, and phase diagram, vary among different families of cuprates. In terms of the phase diagram, previous studies on  $\text{YBa}_2\text{Cu}_3\text{O}_7$  [11–13,24],  $\text{La}_{2-x}\text{Ba}_x\text{CuO}_4$  [8,9], and  $\text{La}_{1.8-x}\text{Eu}_{0.2}\text{Sr}_x\text{CuO}_{4+\delta}$  [25] show that the CO usually exists within the doping range of the superconducting dome. As doping concentration increases, the critical temperature of the CO increases from low temperature to a maximum value before decreasing, forming a dome-shaped phase diagram [26]. In contrast, x-ray scattering measurements have shown that the  $T_{\text{CO}}$  of  $\text{Bi}_2\text{Sr}_{2-x}\text{La}_x\text{CuO}_{6+\delta}$  (La-Bi2201) decreases monotonically from underdoped ( $T_c = 15$  K,  $p = 0.115$ ) to optimally doped ( $T_c = 33$  K,  $p = 0.16$ ) [15,16] [Fig. 1(a)]. Whether the CO in La-Bi2201 deviates from a dome-shaped behavior requires the study of lower-doped samples.

Bi-based cuprates provide a suitable platform to study the emergence and evolution of CO, as a broad doping range spanning the entire phase diagram from Mott insulators to Fermi liquids can be obtained through doping with Pb, La, or oxygen [27–30]. Furthermore, the easy cleavage of Bi-based cuprates allows measurements to be made using surface-sensitive techniques such as scanning tunneling microscope (STM) and angle-resolved photoemission spectroscopy (ARPES). Previous STM studies have revealed chequerboard patterns in extremely low-doped Bi2201 at liquid-helium temperatures, indicating that chequerboard charge order is present in an insulating sample with  $p = 0.07$ , but absent in a

\*These authors contributed equally to this work.

†Present Address: Shenzhen Pinghu Laboratory, Shenzhen 518111, China.

‡Contact author: [yingying.peng@pku.edu.cn](mailto:yingying.peng@pku.edu.cn)

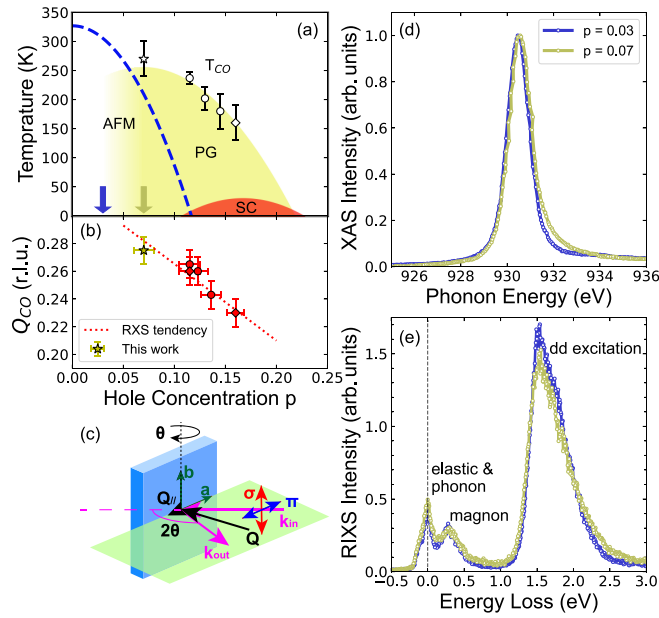


FIG. 1. (a) The phase diagram of Bi2201, including antiferromagnetism (AFM), pseudogap (PG), and superconductivity (SC) [34,35]. The arrows indicate two dopings measured in our work. The circle [15] and diamond [16] markers represent the onset temperatures of the CO ( $T_{CO}$ ) obtained from previous studies, and the star marker indicates the finding from this work. (b) Doping dependence of the wave vector of CO obtained by resonant x-ray scattering (RXS) (red), with data from this work (star), Ref. [15] (circle), and Ref. [16] (diamond). The dashed lines are guides to the eye. (c) Schematic diagram of our experimental geometry. (d) The total fluorescence yield (TFY) x-ray absorption spectroscopy (XAS) of two samples measured at Cu  $L_3$  edge and taken at normal incidence. They are normalized to the resonance of the main peak. (e) RIXS spectra at  $Q_{\parallel} = (0.4, 0)$  measured with a  $\pi$ -polarized incident beam. The intensity was normalized by  $dd$  excitation. Note that the shoulder at  $\sim -0.1$  eV is due to an instrumental issue, which affects only the energy gain side for the  $\pi$ -polarized spectra.

more insulating sample with  $p = 0.03$  [31]. More recently, it has been observed that the  $p = 0.08$  sample is not uniformly doped, containing both undoped antiferromagnetic regions and slightly doped charge-ordered regions, which coincide with the preformed pseudogap region [32]. STM measurements have also found that Cooper pairs form in these localized charge-ordered regions, with the antiferromagnetic regions eventually disappearing and the charge-ordered regions becoming interconnected as doping reaches the onset of superconductivity ( $p = 0.1$ ) [33]. Despite the rich nanoscale electronic inhomogeneity revealed by STM, it remains unclear how charge order evolves with temperature, as high-temperature experiments pose challenges due to thermal drift. Furthermore, STM is a surface-sensitive technique, raising questions about the existence of bulk charge order in extremely underdoped La-Bi2201. Therefore, a bulk-sensitive technique covering a wide temperature range is needed to study how COs emerge and evolve with increasing doping.

In this paper we have performed Cu  $L_3$ -edge ( $\sim 931$  eV) resonant inelastic x-ray spectroscopy (RIXS) measurements on extremely underdoped  $\text{Bi}_2\text{Sr}_{2-x}\text{La}_x\text{CuO}_{6+\delta}$  (La-Bi2201)

samples with doping levels of  $p = 0.03$  and  $p = 0.07$ . The results show that CO exists in the  $p = 0.07$  sample with a wave vector of  $Q_{CO} = (0.275, 0)$  and a coherence length of  $\xi = 3a_0$ . The observed wave vector follows the trend extrapolated from higher doping samples determined by x-ray scattering experiments. The coherence length corresponds to a wave-packet length of  $2\pi\xi \sim 7$  nm in real space, consistent with the high charge density region observed by STM. We also found that the CO weakens at higher temperatures, similar to the behavior of CO in higher-doped Bi2201 [15,16]. Furthermore, no CO signal was observed in the  $p = 0.03$  sample. Our work indicates that the CO in Bi2201 forms a truncated dome-shaped phase diagram, which arises from the nanoscale inhomogeneity of Bi2201 at low doping levels. Since the CO in inhomogeneous systems is established in localized high charge density regions, the reduction and disappearance of these regions at lower doping levels lead to the disappearance of the CO. This results in a truncated phase diagram for COs at a finite transition temperature. Our results reveal how CO emerges from extremely underdoped regions in inhomogeneous systems such as Bi2201.

## II. EXPERIMENTS AND RESULTS

High-quality  $\text{Bi}_2\text{Sr}_{2-x}\text{La}_x\text{CuO}_{6+\delta}$  single crystals were grown by the traveling solvent floating zone method as described in Refs. [30,34]. By doping La to  $x = 0.84$  and  $1.1$ , we obtained two insulating samples with hole doping levels of  $p = 0.03$  and  $p = 0.07$  [Fig. 1(a)]. The lattice was defined by a pseudotetragonal unit cell with lattice parameters  $a = b = 3.8$  Å, and  $c = 23.8$  Å for the  $p = 0.03$  sample, and  $c = 24.0$  Å for the  $p = 0.07$  sample (see Fig. 5 in the Appendix). The cleaved surface of our sample was the  $ab$  plane. The RIXS experiments were performed at beamline 41A at the National Synchrotron Radiation Research Center (NSRRC) [36]. The incident photon energy was tuned to the resonance of the Cu  $L_3$  edge, with an energy resolution of  $\sim 90$  meV. The scattering plane was horizontal, spanned by the incident and outgoing beams [Fig. 1(c)]. The scattering angle was fixed at  $150^\circ$ , and the RIXS spectra were collected with a  $\sigma$ -polarized incident beam unless otherwise stated. By varying the angle  $\theta$ , we can change the projection of momentum transfer  $\mathbf{Q}$  within the  $ab$  plane ( $Q_{\parallel}$ ). Each RIXS spectrum was collected for 30 min (sum of six individual spectra).

The x-ray absorption spectra (XAS) of two samples are displayed in Fig. 1(d). The  $p = 0.07$  sample exhibits a broader  $[2p3d^9L]$  tail resulting from the hybridization of Cu  $3d$  and O  $2p$  orbitals [37]. The RIXS spectra measured with  $\pi$  polarization at  $Q_{\parallel} = (0.4, 0)$  are shown in Fig. 1(e), consisting of an elastic peak, phonons ( $< 0.1$  eV), a paramagnon ( $\sim 0.2$ – $0.5$  eV), and  $dd$  excitations ( $\sim 1$ – $3$  eV). The sharper paramagnon peak in the  $p = 0.03$  sample suggests it is closer to the antiferromagnetic (AFM) phase [38].

To enhance the charge scattering signals, we employed  $\sigma$  polarization to investigate the RIXS spectra along the  $(H, 0)$  direction at 23 K. The energy-momentum intensity maps after  $dd$  normalization are presented in Figs. 2(a) and 2(c). For the  $p = 0.07$  sample, a symmetric peak was observed on both the  $(H, 0)$  and  $(-H, 0)$  sides, while no peak was found for the  $p = 0.03$  sample. Notably, the quasielastic peak within

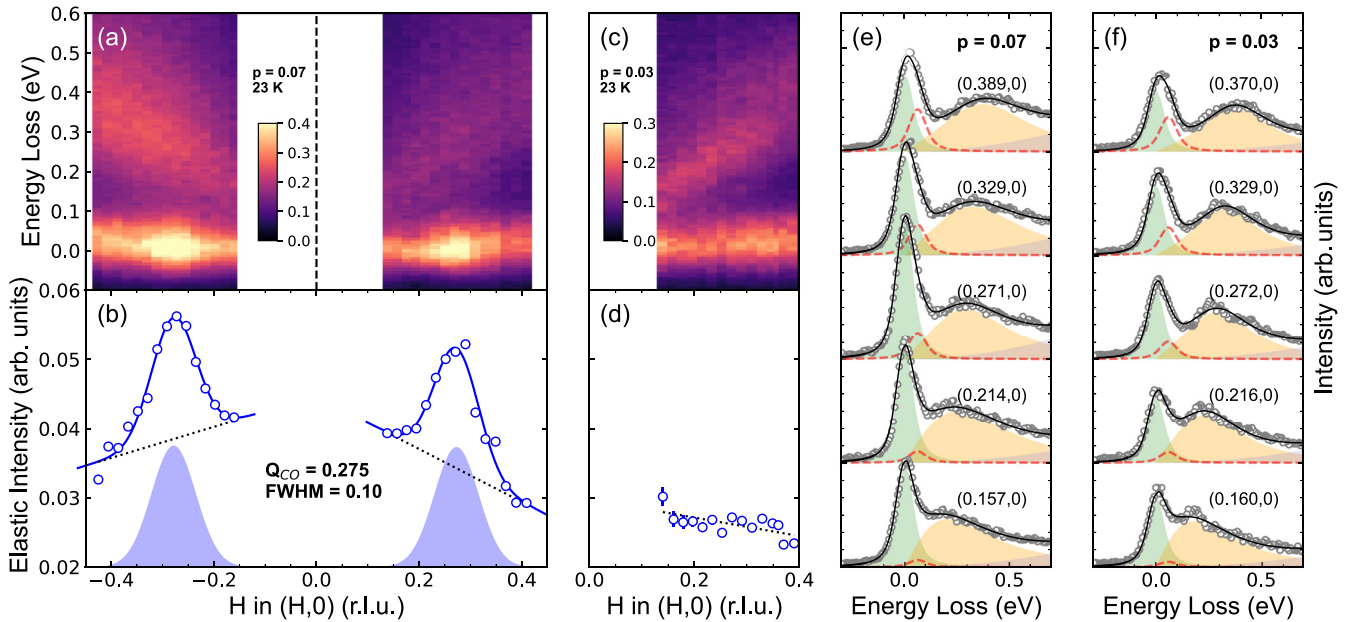


FIG. 2. (a), (c) The energy-momentum intensity maps of  $p = 0.07$  and  $p = 0.03$  samples, respectively. The RIXS spectra were collected at 23 K with a  $\sigma$ -polarized incident beam and were normalized by  $dd$  excitation. A CO peak is observed at both  $(H, 0)$  and  $(-H, 0)$  sides in the  $p = 0.07$  sample. (b), (d) The  $H$  dependence of extracted elastic peak intensity after fitting the RIXS spectra. In the  $p = 0.07$  sample,  $Q_{CO} = 0.275$  and the coherence length is  $\sim 3a_0$ . (e), (f) Fit of RIXS spectra of the  $p = 0.07$  and  $p = 0.03$  sample, including elastic peak (green peak), phonons (dashed line), paramagnon (yellow peak), and background from  $dd$  excitation (purple tail).

this map includes phonon contributions that become more pronounced at larger momentum transfer. A separation from the phonon contribution is required to accurately determine the intensity of the elastic peak over different momenta. Due to the limited energy resolution, the simultaneous extraction of phonon energy and intensity by fitting our RIXS spectra is not feasible. Therefore, we refer to a previous study of Bi2201 using an approximate phonon energy of 60 meV [39]. We can extract the phonon intensity by fixing the phonon energy to 60 meV (see Fig. 6 in the Appendix). Here, we utilized two Voigt functions of equal width to fit the elastic peak and phonons, an antisymmetric Lorentz function for the paramagnon [38] and a quadratic polynomial for the  $dd$  tail. Examples of the fitting results and the extracted intensity of the elastic peak are presented in Figs. 2(e) and 2(f). The fitted momentum-dependent intensity of the elastic peaks is shown in Figs. 2(b) and 2(d).

We employed a Gaussian function and a linear background to further extract the wave vector and full width at half maximum (FWHM) of the peak of the  $p = 0.07$  sample [Fig. 2(b)]. The wave vector is determined to be  $(0.275, 0)$ , following the extrapolated trend of the CO in higher-doped Bi2201 observed by resonant x-ray scattering (RXS) [15,16]. In contrast, a previous STM study observed a wave vector of 0.25 in extremely underdoped Bi2201 [31]. The incommensurate CO detected by RIXS is proposed to manifest in real space as a series of patterns of localized commensurate CO with monotonic phase shifts [40]. However, our experiment without phase sensitivity cannot directly address this discrepancy. The FWHM is determined to be 0.10 r.l.u. Following the general definition

$\xi_a = a/(\pi \times \text{FWHM})$  [41], the coherence length of the peak is estimated to be  $\xi \sim 3a_0$  in the  $p = 0.07$  sample, which is comparable to previous x-ray scattering results of CO in underdoped La-Bi2201 ( $4.5a_0$ – $6.0a_0$ ) [15,16]. Although  $\xi$  is relatively short, the CO is well-defined because the average length of the real-space wave packet is  $2\pi\xi \sim 19a_0$ , which is longer than the wavelength ( $\sim 4a_0$ ). This wave-packet length is consistent with the scale of the local CO islands observed in similarly doped samples by STM experiments [32]. This suggests that the short coherence length arises from the electronic inhomogeneity in extremely underdoped Bi2201 [32]. In contrast, for the  $p = 0.03$  sample, the intensity of the elastic peak shows a linear background without any peak.

To study the temperature dependence of the CO, we also measured RIXS spectra of the  $p = 0.07$  sample at 100 and 200 K. The energy-momentum maps shown in Figs. 3(a)–3(c) show that the CO becomes weaker at higher temperatures while the paramagnon is temperature independent [Fig. 3(d)]. For the elastic peak, we obtained the  $H$  dependence of its intensity at different temperatures, which can be fitted by a Gaussian peak on a linear background [Fig. 3(e)]. As the temperature increases, the  $Q_{CO}$  does not change, and only the intensity weakens. Since both the temperature dependence of the intensity and the wave vector in extremely underdoped Bi2201 are more consistent with the behavior of CO in higher-doped Bi2201 [15], we suggest that the peak in the  $p = 0.07$  sample has the same nature as the CO observed in higher-doped Bi2201. By applying the same linear fitting method used for higher-doped Bi2201 [15], we estimate the transition temperature to be approximately 270 K [Fig. 3(f)].

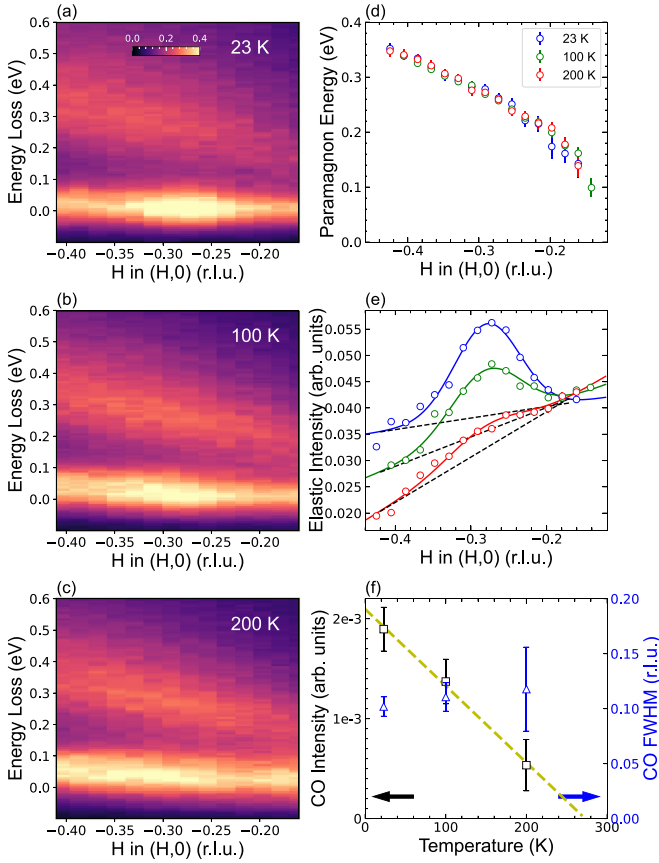


FIG. 3. (a)–(c) The energy-momentum intensity maps of the  $p = 0.07$  sample at 23, 100, and 200 K. The CO peak becomes weaker and broader at higher temperatures. (d) The dispersion of the paramagnon was obtained by fitting the RIXS spectra, which remains unchanged at different temperatures. (e) The  $H$  dependence of extracted elastic peak intensity at different temperatures. (f) Temperature dependence of the intensity of CO, implying CO disappears above 270 K.

### III. DISCUSSION

Combining the temperature dependence and the doping dependence, we then discuss how the CO evolves in this system. It is thought-provoking why the  $p = 0.07$  sample has such a high critical temperature of CO, but the  $p = 0.03$  sample has no CO even at low temperatures. According to a widely known copper-oxygen phase diagram [1], a dome-shaped CO phase is typically expected. However, our findings reveal that in extremely underdoped Bi2201, the CO emerges at high temperatures. When combined with results from more highly doped Bi2201 [15,16], the CO phase forms a truncated dome-shaped diagram, as illustrated in Fig. 1(a).

This truncated dome-shaped phase diagram may arise from the electronic inhomogeneity observed in Bi2201. A previous STM study on extremely underdoped Bi2201 ( $p = 0.08$ ) showed that charge order and antiferromagnetic order appear in distinct regions, with the carrier density being higher in the CO regions compared to the antiferromagnetic ones [32]. We use a schematic representation to illustrate this scenario, as shown in Fig. 4(a). We assume that charge order forms when the local charge density exceeds a threshold  $p_c$ , highlighted in

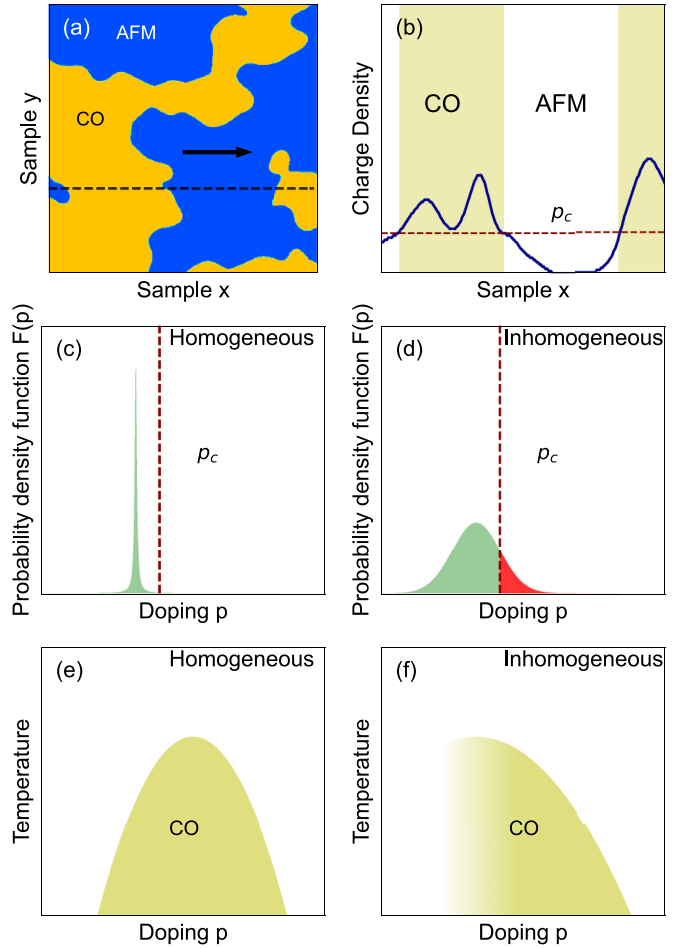


FIG. 4. (a) A schematic representation illustrating the localized formation of CO islands, inspired by STM observations [32]. This plot reflects the spatial distribution and inhomogeneous nature of the charge density, where the area of the CO is separated from the area of the AFM. (b) A schematic of a charge density along the cut marked by a gray dashed line in (a).  $p_c$  represents the critical doping for the formation of charge order, while the yellow region represents the region where the CO was formed. (c) The probability density function for the homogeneous sample. All the local charge densities are below  $p_c$ . (d) The probability density function for the inhomogeneous sample. Some portions of the sample have a larger charge density than  $p_c$  and form CO. (e) The dome-like CO phase diagram in the homogeneous system with well-defined onset doping. (f) The schematic phase diagram of CO in the inhomogeneous system.

the yellow region of Fig. 4(b). Here, we use the probability density function (PDF) of charge density, which describes the statistical distribution of different charge density regions, to discuss the critical phase transition behavior. For a homogeneous sample, the PDF of charge density can be approximated as a narrow peak [Fig. 4(c)]. Adjusting the average doping shifts the peak's center; when this peak crosses the  $p_c$  line, the entire sample simultaneously develops charge order, showing a distinct onset doping behavior. This leads to a well-defined critical doping, resulting in a dome-shaped phase diagram, as depicted in Fig. 4(e).

In contrast, for an inhomogeneous sample, the PDF of charge density forms a broader peak, and charge order

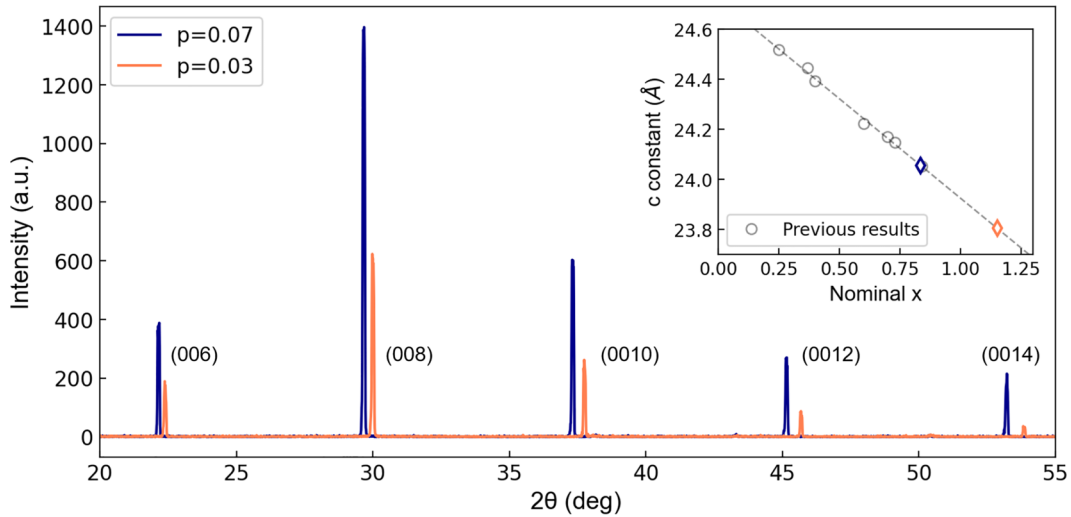


FIG. 5. High-resolution XRD measurements along the  $c$  axis using a monochromatic Cu  $K\alpha$  source. The indices are provided next to the Bragg peaks. The inset shows that our results (diamond markers) follow the trend of the  $c$  lattice constant of previous results (gray circles) [30].

emerges locally in charge-abundant regions, represented in red in Fig. 4(d). In this case, the charge order does not exhibit a well-defined critical doping behavior. Instead, as doping decreases, the high charge density regions shrink, weakening the CO intensity and shortening the coherence length until the CO disappears entirely. This leads to the disappearance of the CO at finite temperatures, corresponding to the decreasing coherence length, and results in a truncated phase diagram, as shown in Fig. 4(f). This picture for an inhomogeneous system is consistent with evolution of the CO observed in La-Bi2201. Notably, STM studies also report nanoscale electronic inhomogeneities in bilayer cuprate  $\text{Bi}_2\text{Sr}_2\text{CaCu}_2\text{O}_{8+\delta}$  (Bi2212) [42]. Thus, further exploration of CO evolution in underdoped Bi2212 could assess the broader applicability of the connection between inhomogeneities and the truncated dome phase diagram. Additionally, inhomogeneity might explain the recently observed truncated CO dome phase diagram in Pr-doped  $\text{YBa}_2\text{Cu}_3\text{O}_{7-y}$  films grown on  $(\text{LaAlO}_3)_{0.3}(\text{Sr}_2\text{TaAlO}_6)_{0.7}$  (LSAT) substrates [43].

#### IV. CONCLUSIONS

In summary, we report the evolution of CO in extremely underdoped La-Bi2201 with hole doping levels of  $p = 0.03$  and  $p = 0.07$  using Cu  $L$ -edge RIXS. Our results show that bulk CO is absent at  $p = 0.03$  and appears at  $p = 0.07$ . The temperature dependence of the intensity and the wave vector of the CO at  $p = 0.07$  samples suggest a consistent nature with the CO observed in higher-doped samples [15,16]. The appearance of the CO from  $p = 0.03$  to  $p = 0.07$  deviates from a domelike behavior in the phase diagram. Considering previous STM results on extremely underdoped La-Bi2201, we suggest that such a truncated dome-shaped phase diagram arises from the inhomogeneity of the system. Our findings thus provide valuable insight into the relationship between microscopic nanoscale inhomogeneities and the macroscopic behavior observed in the phase diagram.

#### ACKNOWLEDGMENTS

Y.Y.P. is grateful for financial support from the Ministry of Science and Technology of China (Grants No. 2019YFA0308401 and No. 2021YFA1401903), the National Natural Science Foundation of China (Grants No. 12374143 and No. 11974029), and Beijing Natural Science Foundation (Grant No. JQ24001). X.J.Z.'s work is supported by the National Key Research and Development Program of China (Grant No. 2021YFA1401800). The RIXS experimental data were collected at beamline 41A of the National Synchrotron

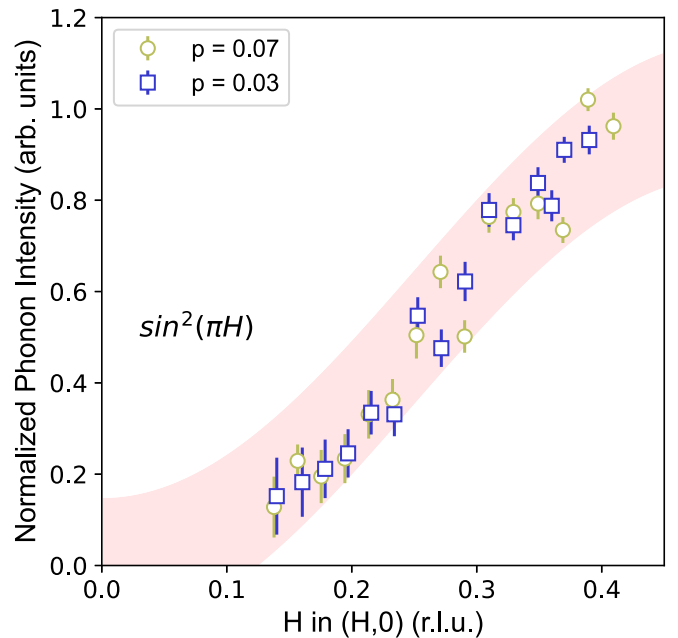


FIG. 6. The  $H$  dependence of phonon peak intensity from the fitting results of Figs. 2(e) and 2(f). Both phonons of  $p = 0.03$  and  $p = 0.07$  samples followed the  $\sin^2(\pi H)$  along the  $(H, 0)$  direction.

TABLE I. The relative content of compositions in La-Bi2201 estimated from EDS, normalized to Cu.

Hole doping	Nominal composition	Measured composition	$c$ (Å)
0.07	$\text{Bi}_2\text{Sr}_{1.16}\text{La}_{0.84}\text{CuO}_{6+\delta}$	$\text{Bi}_{2.04}\text{Sr}_{0.95}\text{La}_{0.89}\text{CuO}_{6+\delta}$	$24.056 \pm 0.005$
0.03	$\text{Bi}_2\text{Sr}_{0.90}\text{La}_{1.10}\text{CuO}_{6+\delta}$	$\text{Bi}_{2.03}\text{Sr}_{0.79}\text{La}_{1.15}\text{CuO}_{6+\delta}$	$23.815 \pm 0.005$

Radiation Research Center (NSRRC) in Hsinchu 30076, Taiwan.

## APPENDIX

### 1. Sample preparation and characterization

The  $\text{Bi}_2\text{Sr}_{2-x}\text{La}_x\text{CuO}_{6+\delta}$  (La-Bi2201) single crystals were grown by the traveling solvent floating zone method [30]. By annealing in the atmosphere for different La-doped samples, we obtained different hole-doped samples. The nominal La concentrations are 1.1 and 0.84, corresponding to  $p = 0.03$  and 0.07, respectively, as referenced from previous studies [34]. We verified the concentration of La doping in our samples by high-resolution x-ray diffraction (HRXRD) and energy dispersive x-ray spectroscopy (EDS). The results, listed in Table I, are consistent with the nominal values within the margin of error.

Our EDS measurements were carried on an Oxford X-Max 80 EDS accessorized in an FEI Helios NanoLab 600i Dual-Beam System. We used an electron beam with an accelerating energy of 30 keV to measure three  $50 \mu\text{m} \times 50 \mu\text{m}$  areas for each sample. The measured La concentrations are  $0.89 \pm 0.03$  for the  $p = 0.07$  sample and  $1.15 \pm 0.04$  for the  $p = 0.03$  sample.

HRXRD data were collected using a monochromatic Cu  $K\alpha$  source on a 1.6-kW high-resolution Bruker Discover-8 system. We have observed a series of Bragg peaks along the (001) direction (Fig. 5), and calculated the  $c$  lattice constants as  $24.056 \pm 0.005$  and  $23.815 \pm 0.005$  Å, respectively. According to the dependence of the  $c$  lattice constant with La doping established in the literature [30], the La element ( $x$ ) in our two samples are estimated as  $0.84 \pm 0.01$  and  $1.14 \pm 0.01$ , which are close to our nominal values.

The temperature dependence of resistivity for the same batch of  $\text{Bi}_2\text{Sr}_{2-x}\text{La}_x\text{CuO}_{6+\delta}$  samples was reported in a prior study [34]. The  $x = 1.1$  sample is more insulating than the  $x = 0.84$  sample. The resistivity-temperature ( $\rho$ - $T$ ) curves of the La-Bi2201 single crystals with low doping levels of  $p = 0.03$  and  $p = 0.08$  samples follow the behavior of  $\rho = \rho_0 e^{(T_0/T)^{1/3}}$ , consistent with the model of two-dimensional (2D) variable-range hopping of localized charges.

### 2. Fit result of phonon intensity

To separate the elastic peak from the phonon peaks in our RIXS spectra, we used the fitting method described in the main text. The results of the phonon intensity show a  $\sin^2(\pi H)$  dependence, as plotted in Fig. 6.

- [1] B. Keimer, S. A. Kivelson, M. R. Norman, S. Uchida, and J. Zaanen, From quantum matter to high-temperature superconductivity in copper oxides, *Nature (London)* **518**, 179 (2015).
- [2] P. A. Lee, N. Nagaosa, and X.-G. Wen, Doping a Mott insulator: Physics of high-temperature superconductivity, *Rev. Mod. Phys.* **78**, 17 (2006).
- [3] S. A. Kivelson, I. P. Bindloss, E. Fradkin, V. Oganesyan, J. M. Tranquada, A. Kapitulnik, and C. Howald, How to detect fluctuating stripes in the high-temperature superconductors, *Rev. Mod. Phys.* **75**, 1201 (2003).
- [4] E. Weckert, The potential of future light sources to explore the structure and function of matter, *IUCr J* **2**, 230 (2015).
- [5] J. M. Tranquada, B. J. Sternlieb, J. D. Axe, Y. Nakamura, and S. Uchida, Evidence for stripe correlations of spins and holes in copper oxide superconductors, *Nature (London)* **375**, 561 (1995).
- [6] M. Fujita, H. Goka, K. Yamada, and M. Matsuda, Competition between charge- and spin-density-wave order and superconductivity in  $\text{La}_{1.875}\text{Ba}_{0.125-x}\text{Sr}_x\text{CuO}_4$ , *Phys. Rev. Lett.* **88**, 167008 (2002).
- [7] H. Kimura, H. Goka, M. Fujita, Y. Noda, K. Yamada, and N. Ikeda, Synchrotron x-ray diffraction study of a charge stripe order in  $\frac{1}{8}$ -doped  $\text{La}_{1.875}\text{Ba}_{0.125-x}\text{Sr}_x\text{CuO}_4$ , *Phys. Rev. B* **67**, 140503(R) (2003).
- [8] P. Abbamonte, A. Rusydi, S. Smadici, G. D. Gu, G. A. Sawatzky, and D. L. Feng, Spatially modulated ‘Mottness’ in  $\text{La}_{2-x}\text{Ba}_x\text{CuO}_4$ , *Nat. Phys.* **1**, 155 (2005).
- [9] M. Hücker, M. v. Zimmermann, G. D. Gu, Z. J. Xu, J. S. Wen, G. Xu, H. J. Kang, A. Zheludev, and J. M. Tranquada, Stripe order in superconducting  $\text{La}_{2-x}\text{Ba}_x\text{CuO}_4$  ( $0.095 \leq x \leq 0.155$ ), *Phys. Rev. B* **83**, 104506 (2011).
- [10] T. Wu, H. Mayaffre, S. Krämer, M. Horvatić, C. Berthier, W. N. Hardy, R. Liang, D. A. Bonn, and M.-H. Julien, Magnetic-field-induced charge-stripe order in the high-temperature superconductor  $\text{YBa}_2\text{Cu}_3\text{O}_{6+y}$ , *Nature (London)* **477**, 191 (2011).
- [11] G. Ghiringhelli, M. Le Tacon, M. Minola, S. Blanco-Canosa, C. Mazzoli, N. B. Brookes, G. M. De Luca, A. Frano, D. G. Hawthorn, F. He *et al.*, Long-range incommensurate charge fluctuations in  $(\text{Y,Nd})_2\text{Cu}_3\text{O}_{6+x}$ , *Science* **337**, 821 (2012).
- [12] A. J. Achkar, R. Sutarto, X. Mao, F. He, A. Frano, S. Blanco-Canosa, M. Le Tacon, G. Ghiringhelli, L. Braicovich, M. Minola *et al.*, Distinct charge orders in the planes and chains of ortho-III-ordered  $\text{YBa}_2\text{Cu}_3\text{O}_{6+\delta}$  superconductors identified by resonant elastic x-ray scattering, *Phys. Rev. Lett.* **109**, 167001 (2012).
- [13] E. Blackburn, J. Chang, M. Hücker, A. T. Holmes, N. B. Christensen, R. Liang, D. A. Bonn, W. N. Hardy, U. Rütt, O. Gutowski *et al.*, X-ray diffraction observations of a charge-density-wave order in superconducting ortho-II  $\text{YBa}_2\text{Cu}_3\text{O}_{6.54}$

- single crystals in zero magnetic field, *Phys. Rev. Lett.* **110**, 137004 (2013).
- [14] J. Chang, E. Blackburn, O. Ivashko, A. T. Holmes, N. B. Christensen, M. Hücker, R. Liang, D. A. Bonn, W. N. Hardy, U. Rütt *et al.*, Magnetic field controlled charge density wave coupling in underdoped  $\text{YBa}_2\text{Cu}_3\text{O}_{6+x}$ , *Nat. Commun.* **7**, 11494 (2016).
- [15] R. Comin, A. Frano, M. M. Yee, Y. Yoshida, H. Eisaki, E. Schierle, E. Weschke, R. Sutarto, F. He, A. Soumyanarayanan *et al.*, Charge order driven by Fermi-arc instability in  $\text{Bi}_2\text{Sr}_{2-x}\text{La}_x\text{CuO}_{6+\delta}$ , *Science* **343**, 390 (2014).
- [16] Y. Y. Peng, M. Salluzzo, X. Sun, A. Ponti, D. Betto, A. M. Ferretti, F. Fumagalli, K. Kummer, M. Le Tacon, X. J. Zhou *et al.*, Direct observation of charge order in underdoped and optimally doped  $\text{Bi}_2(\text{Sr}, \text{La})_2\text{CuO}_{6+\delta}$  by resonant inelastic x-ray scattering, *Phys. Rev. B* **94**, 184511 (2016).
- [17] E. H. da Silva Neto, P. Aynajian, A. Frano, R. Comin, E. Schierle, E. Weschke, A. Gyenis, J. Wen, J. Schneeloch, Z. Xu *et al.*, Ubiquitous interplay between charge ordering and high-temperature superconductivity in cuprates, *Science* **343**, 393 (2014).
- [18] M. Hashimoto, G. Ghiringhelli, W.-S. Lee, G. Dellea, A. Amorese, C. Mazzoli, K. Kummer, N. B. Brookes, B. Moritz, Y. Yoshida *et al.*, Direct observation of bulk charge modulations in optimally doped  $\text{Bi}_{1.5}\text{Pb}_{0.6}\text{Sr}_{1.54}\text{CaCu}_2\text{O}_{8+\delta}$ , *Phys. Rev. B* **89**, 220511(R) (2014).
- [19] W. Tabis, Y. Li, M. L. Tacon, L. Braicovich, A. Kreyssig, M. Minola, G. Dellea, E. Weschke, M. J. Veit, M. Ramazanoglu *et al.*, Charge order and its connection with Fermi-liquid charge transport in a pristine high- $T_c$  cuprate, *Nat. Commun.* **5**, 5875 (2014).
- [20] J. Chang, E. Blackburn, A. T. Holmes, N. B. Christensen, J. Larsen, J. Mesot, R. Liang, D. A. Bonn, W. N. Hardy, A. Watenphul *et al.*, Direct observation of competition between superconductivity and charge density wave order in  $\text{YBa}_2\text{Cu}_3\text{O}_{6.67}$ , *Nat. Phys.* **8**, 871 (2012).
- [21] S. Gerber, H. Jang, H. Nojiri, S. Matsuzawa, H. Yasumura, D. A. Bonn, R. Liang, W. N. Hardy, Z. Islam, A. Mehta *et al.*, Three-dimensional charge density wave order in  $\text{YBa}_2\text{Cu}_3\text{O}_{6.67}$  at high magnetic fields, *Science* **350**, 949 (2015).
- [22] W. S. Lee, K.-J. Zhou, M. Hepting, J. Li, A. Nag, A. C. Walters, M. Garcia-Fernandez, H. C. Robarts, M. Hashimoto, H. Lu *et al.*, Spectroscopic fingerprint of charge order melting driven by quantum fluctuations in a cuprate, *Nat. Phys.* **17**, 53 (2021).
- [23] H. Jang, S. Song, T. Kihara, Y. Liu, S.-J. Lee, S.-Y. Park, M. Kim, H.-D. Kim, G. Coslovich, S. Nakata *et al.*, Characterization of photoinduced normal state through charge density wave in superconducting  $\text{YBa}_2\text{Cu}_3\text{O}_{6.67}$ , *Sci. Adv.* **8**, eabk0832 (2022).
- [24] M. Hücker, N. B. Christensen, A. T. Holmes, E. Blackburn, E. M. Forgan, R. Liang, D. A. Bonn, W. N. Hardy, O. Gutowski, M. v. Zimmermann *et al.*, Competing charge, spin, and superconducting orders in underdoped  $\text{YBa}_2\text{Cu}_3\text{O}_y$ , *Phys. Rev. B* **90**, 054514 (2014).
- [25] J. Fink, V. Soltwisch, J. Geck, E. Schierle, E. Weschke, and B. Büchner, Phase diagram of charge order in  $\text{La}_{1.8-x}\text{Eu}_{0.2}\text{Sr}_x\text{CuO}_4$  from resonant soft x-ray diffraction, *Phys. Rev. B* **83**, 092503 (2011).
- [26] R. Comin and A. Damascelli, Resonant x-ray scattering studies of charge order in cuprates, *Annu. Rev. Condens. Matter Phys.* **7**, 369 (2016).
- [27] A. Maeda, M. Hase, I. Tsukada, K. Noda, S. Takebayashi, and K. Uchinokura, Physical properties of  $\text{Bi}_2\text{Sr}_2\text{Ca}_{n-1}\text{Cu}_n\text{O}_y$  ( $n = 1, 2, 3$ ), *Phys. Rev. B* **41**, 6418 (1990).
- [28] N. L. Wang, Y. Chong, C. Y. Wang, D. J. Huang, Z. Q. Mao, L. Z. Cao, and Z. J. Chen, Doping dependence of normal-state transport properties in La- and Pb-doped  $\text{Bi}_2\text{Sr}_2\text{CuO}_y$ , *Phys. Rev. B* **47**, 3347 (1993).
- [29] T. Yasuda, S. Takano, and L. Rinderer, Effects of oxygen non-stoichiometry on the anisotropic resistivity in  $\text{Bi}_2\text{Sr}_2\text{CaCu}_2\text{O}_{8+x}$ , *Physica C: Superconductivity* **208**, 385 (1993).
- [30] J. Meng, G. Liu, W. Zhang, L. Zhao, H. Liu, W. Lu, X. Dong, and X. J. Zhou, Growth, characterization and physical properties of high-quality large single crystals of  $\text{Bi}_2(\text{Sr}_{2-x}\text{La}_x)\text{CuO}_{6+\delta}$  high-temperature superconductors, *Supercond. Sci. Technol.* **22**, 045010 (2009).
- [31] P. Cai, W. Ruan, Y. Peng, C. Ye, X. Li, Z. Hao, X. Zhou, D.-H. Lee, and Y. Wang, Visualizing the evolution from the Mott insulator to a charge-ordered insulator in lightly doped  $\text{A}$  cuprates, *Nat. Phys.* **12**, 1047 (2016).
- [32] H. Li, H. Li, Z. Wang, S. Wan, H. Yang, and H.-H. Wen, Low-energy gap emerging from confined nematic states in extremely underdoped cuprate superconductors, *npj Quantum Mater.* **8**, 18 (2023).
- [33] S. Ye, C. Zou, H. Yan, Y. Ji, M. Xu, Z. Dong, Y. Chen, X. Zhou, and Y. Wang, The emergence of global phase coherence from local pairing in underdoped cuprates, *Nat. Phys.* **19**, 1301 (2023).
- [34] Y. Peng, J. Meng, D. Mou, J. He, L. Zhao, Y. Wu, G. Liu, X. Dong, S. He, J. Zhang *et al.*, Disappearance of nodal gap across the insulator-superconductor transition in a copper-oxide superconductor, *Nat. Commun.* **4**, 2459 (2013).
- [35] S. Kawasaki, C. Lin, P. L. Kuhns, A. P. Reyes, and G.-q. Zheng, Carrier-concentration dependence of the pseudogap ground state of superconducting  $\text{Bi}_2\text{Sr}_{2-x}\text{La}_x\text{CuO}_{6+\delta}$  revealed by  $^{63,65}\text{Cu}$ -nuclear magnetic resonance in very high magnetic fields, *Phys. Rev. Lett.* **105**, 137002 (2010).
- [36] A. Singh, H. Y. Huang, Y. Y. Chu, C. Y. Hua, S. W. Lin, H. S. Fung, H. W. Shiu, J. Chang, J. H. Li, J. Okamoto *et al.*, Development of the soft x-ray AGM-AGS RIXS beamline at the Taiwan Photon Source, *J. Synchrotron Radiat.* **28**, 977 (2021).
- [37] N. Merrien, F. Studer, G. Poullain, C. Michel, A. Flank, P. Lagarde, and A. Fontaine, Redox mechanisms and density of holes by XAS in the compensated series  $\text{Bi}_{2-x}\text{Pb}_x\text{Sr}_2\text{Ca}_{1-x}\text{Y}_x\text{Cu}_2\text{O}_{8+\delta}$  ( $0 \leq x \leq 1$ ), *J. Solid State Chem.* **105**, 112 (1993).
- [38] Y. Y. Peng, E. W. Huang, R. Fumagalli, M. Minola, Y. Wang, X. Sun, Y. Ding, K. Kummer, X. J. Zhou, N. B. Brookes *et al.*, Dispersion, damping, and intensity of spin excitations in the monolayer  $(\text{Bi,Pb})_2(\text{Sr,L a})_2\text{CuO}_{6+\delta}$  cuprate superconductor family, *Phys. Rev. B* **98**, 144507 (2018).
- [39] J. Li, A. Nag, J. Pellicciari, H. Robarts, A. Walters, M. Garcia-Fernandez, H. Eisaki, D. Song, H. Ding, S. Johnston *et al.*, Multiorbital charge-density wave excitations and concomitant phonon anomalies in  $\text{Bi}_2\text{Sr}_2\text{LaCuO}_{6+\delta}$ , *Proc. Natl. Acad. Sci. USA* **117**, 16219 (2020).

- [40] A. Mesaros, K. Fujita, S. D. Edkins, M. H. Hamidian, H. Eisaki, S.-i. Uchida, J. C. S. Davis, M. J. Lawler, and E.-A. Kim, Commensurate  $4a_0$ -period charge density modulations throughout the  $\text{Bi}_2\text{Sr}_2\text{CaCu}_2\text{O}_{8+x}$  pseudogap regime, *Proc. Natl. Acad. Sci. USA* **113**, 12661 (2016).
- [41] S. Blanco-Canosa, A. Frano, E. Schierle, J. Porras, T. Loew, M. Minola, M. Bluschke, E. Weschke, B. Keimer, and M. Le Tacon, Resonant x-ray scattering study of charge-density wave correlations in  $\text{YBa}_2\text{Cu}_3\text{O}_{6+x}$ , *Phys. Rev. B* **90**, 054513 (2014).
- [42] K. McElroy, J. Lee, J. A. Slezak, D.-H. Lee, H. Eisaki, S. Uchida, and J. C. Davis, Atomic-scale sources and mechanism of nanoscale electronic disorder in  $\text{Bi}_2\text{Sr}_2\text{CaCu}_2\text{O}_{8+x}$ , *Science* **309**, 1048 (2005).
- [43] M. Kang, C. C. Zhang, E. Schierle, S. McCoy, J. Li, R. Sutarto, A. Suter, T. Prokscha, Z. Salman, E. Weschke *et al.*, Discovery of charge order in a cuprate Mott insulator, *Proc. Natl. Acad. Sci. USA* **120**, e2302099120 (2023).